Publication: *J. Am. Chem. Soc.* **2021**, *143*, 15326-15334. DOI: 10.1021/jacs.1c06865

Ligand-sensitized Near-infrared to Visible Linear Light-upconversion in a Discrete Molecular Erbium Complex

Bahman Golesorkhi,[a,b*] Soroush Naseri,[a] Laure Guénée,[c] Inès Taarit,[a] Filipe Alves,[a] Homayoun Nozary,[a] and Claude Piguet[a,*]

[a] *Department of Inorganic and Analytical Chemistry. University of Geneva, 30 quai E. Ansermet CH-1211 Geneva 4 (Switzerland).*

[b] *Department of Chemistry, University of California, Berkeley, Berkeley, California 94720 (United States).*

[c] *Laboratory of Crystallography. University of Geneva, 24 quai E. Ansermet. CH-1211 Geneva 4 (Switzerland).*

[*]Emails: bahman.golesorkhi@berkeley.edu; claude.piguet@unige.ch

---

ABSTRACT: While the low absorption cross section of lanthanide-based upconversion systems, in which the trivalent lanthanides (Ln^{3+}) are responsible for converting low to high energy photons, has restricted their application to intense incident light, the emergence of cascade-sensitization through organic dye antenna capable of broadly harvesting near-infrared light in upconversion nanoparticles (UCNPs) opened new horizons in the field. With the aim of pushing molecular upconversion within the range of practical applications, we show herein how incorporation of a near infrared (NIR) organic dye antenna into the ligand scaffold of a mononuclear erbium coordination complex boosts the upconversion brightness of the molecule to such an extent that low power (0.7 $W \cdot cm^{-2}$) NIR laser excitation of $[\mathbf{L6}Er(hfa)_3]^+$ at 801 nm results in measurable visible upconverted signal in dilute solution ($5 \cdot 10^{-4}$ M) at room temperature. Connecting the NIR dye antenna to the Er^{3+} activator in a single discrete molecule cures the inherent low-efficient metal-based excited state absorption (ESA) mechanism with a powerful indirect sensitization via energy transfer upconversion (ETU) which drastically improves the molecular-based upconverted Er^{3+}-centered visible emission.

Introduction

Since the discovery of linear conversion of low energy photons, mostly from the near infrared (NIR) region, into the visible domain, a phenomenon referred to as upconversion,[1] the open-shell trivalent lanthanides (Ln^{3+}), and trivalent erbium (Er^{3+}) in particular, have been exploited as relays for the sequential pilling up of several photons.[2] However, in order to efficiently promoting the Er^{3+}-centered intermediate excited states into a higher-energy excited level, the non-radiative relaxation pathways have to be suppressed. In this context, the most promising metal-based upconversion systems operate in low-phonon inorganic hosts such as ionic solids or nanoparticles which are doped with Er^{3+} activator.[3] Additionally, the efficiency of upconversion in these systems can be boosted up to two orders of magnitude with the help of optimized peripheral sensitizers, mostly Yb^{3+}, for harvesting photons prior to transfer the accumulated energy onto Er^{3+} activators through energy transfer upconversion (ETU) mechanism.[4] Despite the gain brought by the efficient resonant communication through $Yb(^2F_{5/2}) \rightarrow Er(^4I_{11/2})$ energy transfer process, the upconversion systems harnessing Yb^{3+} as sensitizers next to Er^{3+} activators inherently suffer from the low absorption cross section of f-f transitions.[5] Recently, the latter limitation has been transcended by attachment of organic dye antennas possessing broad absorption bands, the cross sections of which are several orders of magnitude larger than those of f-f transitions, to the surface of upconversion nanoparticles (UCNPs).[6] Despite such improvements in their upconversion efficiency, UCNPs suffer from some drawbacks in terms of synthetic reproducibility and particle size, especially when considering their potential incorporation into molecular devices or biological organisms. In accordance with efforts for bringing down the size of metal-based upconversion systems, the dawn of light upconversion in a discrete molecule could be fairly traced back to the induction of visible upconverted signal in the trinuclear $[CrErCr(\mathbf{L1})_3]^{9+}$ complex (Figure 1a).[7] In this molecule, the two peripheral $[Cr^{III}N_6]$ chromophores act as sensitizers for the indirect sensitization of the central $[Er^{III}N_9]$ activator in order to convert NIR photons into visible (green) light through a molecular ETU mechanism.[7] Interestingly, the d-block

Cr^{3+} sensitizer can be successfully replaced with f-block Er^{3+} in $[(\mathbf{L2}Er)F(Er\mathbf{L2})]^{+}$ (ETU mechanism, Figure 1b)[8] or Yb^{3+} in heterometallic Yb_nEr assemblies.[9]

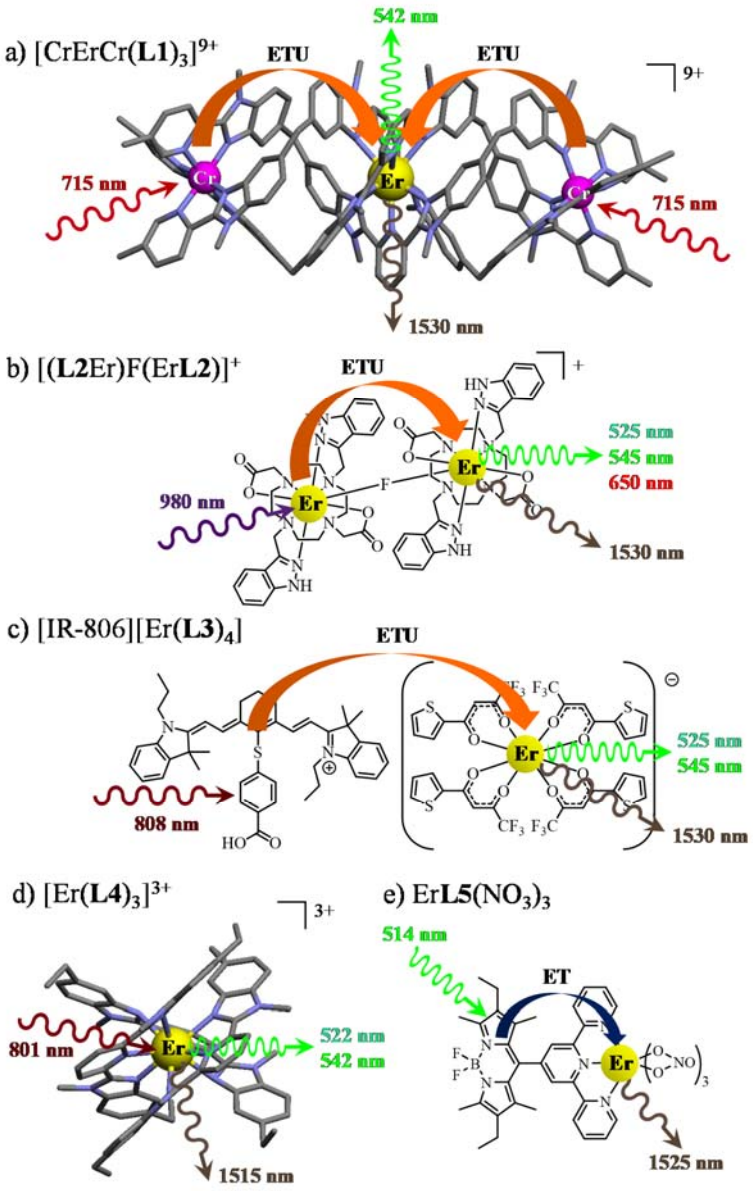

Figure 1. Erbium-based coordination complexes exhibiting a-d) linear upconversion and e) downshifting. The X-ray crystal structures are shown for a) $[CrErCr(\mathbf{L1})_3](CF_3SO_3)_9$ [7] and d) $[Er(\mathbf{L4})_3](ClO_4)_3$.[10a] Chemical structures deduced from spectroscopic data recorded in solution are depicted for b) $[(\mathbf{L2}Er)F(Er\mathbf{L2})]^{+}$,[8] c) [IR-806][Er(**L3**)$_4$] [14] and e) Er**L5**$(NO_3)_3$.[18]

Whatever the choice of metal sensitizers or activators, the intrinsic weak oscillators strengths of the latter d-d or f-f transitions for harvesting the NIR excitation light beam limit the potential gain of ETU in these molecular systems to such an extent that the upconversion quantum yield and brightness

measured for the ETU mechanism operating in trinuclear [CrErCr(**L1**)$_3$]$^{9+}$ are only marginally larger than those observed for the single center ESA mechanism operating in [GaErGa(**L1**)$_3$]$^{9+}$ or in the mononuclear [Er(**L4**)$_3$]$^{3+}$ complex (Figure 1d).[10b] Hence, it is not surprising that the latter drawback urges for the use of high excitation power to sufficiently populate the Ln-centered excited states, which obviously limits the applications of Ln-based molecular upconversion in technologies exploiting solar light since the power density of the terrestrial solar irradiance is approximately 0.1 W·cm^{-2}.[11] Apart from increasing the number of sensitizers per activator unit in a discrete molecular object as craftily demonstrated recently in [Yb$_8$Tb] cluster [12] or in {Er$_2$Yb$_{13}$} aggregate,[13] one alternative remedy to boost the absorptivity of lanthanide coordination complexes may lie in collection of low energy photons through organic dyes located in close proximity of the metallic activator. In an attempt to explore the latter strategy, the erbium-centered visible upconversion was induced in a proposed [IR-806][Er(**L3**)$_4$] ion pair where the intermediate excited levels of Er^{3+} in the anionic [Er(**L3**)$_4$]$^-$ chelate were sensitized by the associated cationic [IR-806]$^+$ NIR dye in anhydrous deuterated chloroform (Figure 1c, neither structural nor thermodynamic characterization is available in solution).[14] Taking into account the dependence of S→A resonance energy transfer rate constants on S-A distances,[15] the unambiguous incorporation of such organic dyes within the ligand structure may significantly improve the efficiency of light upconversion in coordination complexes. Moreover, the replacement of the electrostatic nature of the proposed S-A connection in the ternary [IR-806][Er(**L3**)$_4$] pair with some covalent attachment of the dye antenna to the Er^{3+} activator in a discrete molecule might activate the double-electron exchange (i.e. Dexter) mechanism which requires S-A orbital overlap.[16] Such strategy has been previously employed to generate intense Er^{3+}-centered downshifted emission (i.e., conversion of one photon of high energy into one photon of lower energy) through the '*antenna'* effect[17] in Er(**L5**)(NO$_3$)$_3$, where the connection of a BODIPY-type dye to a 2,2';6',2"-terpyridine binding moiety enhances the molar absorption coefficient of the target discrete molecule in the visible region by several orders of magnitude (Figure 1d).[18] Inspired by these works, we have prepared the cationic sensitizer ligand [**L6**]$^+$, which is equipped with a cyanine antenna for

efficiently harvesting NIR photons. This dye is further covalently connected to a tridentate binding unit for complexing Er^{3+}. Subsequent reaction with $[Er(hfa)_3]^{3+}$ containers quantitatively produces the discrete mononuclear $[\mathbf{L6}Er(hfa)_3]^+$ adduct in solution which boosts NIR to Visible light-upconversion by six orders of magnitudes (Figure 2).

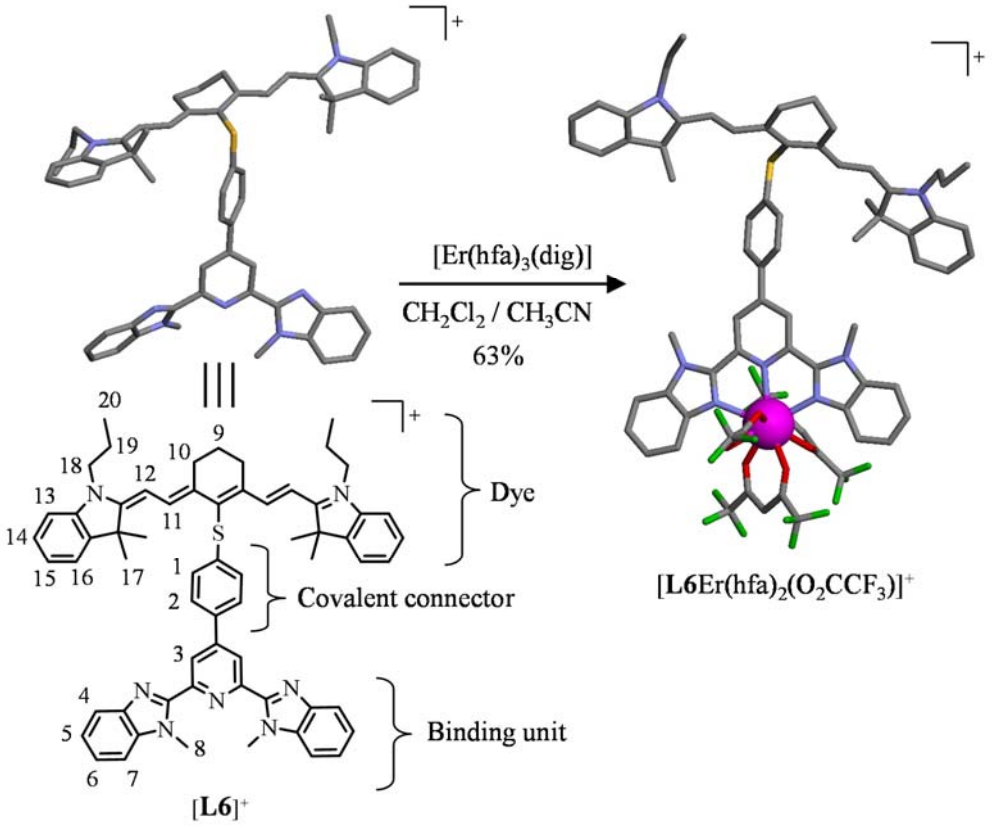

Figure 2. Molecular structures of $[\mathbf{L6}]^+$ ligand (with numbering scheme for NMR) and $[\mathbf{L6}Er(hfa)_2(O_2CCF_3)]^+$ complex taken from the crystal structures of $[\mathbf{L6}](PF_6)$ and $[\mathbf{L6}Er(hfa)_2(O_2CCF_3)](PF_6)\cdot(CH_3CH_2)_2O$. Color code: C, gray; O, red; N, blue; F, green; S, yellow; Er, magenta. H atoms, counter-anions and solvent molecules are omitted for clarity.

Results and Discussion

Synthesis and molecular structures of $[L6]^+$, $[L6Er(hfa)_3]^+$ and $[L6Er(hfa)_2(O_2CCF_3)]^+$. The detailed synthetic procedure as well as the extensive characterizations of the ligand $[\mathbf{L6}]^+$ are described in the supporting information (Scheme S1, Tables S1-S3, Figures S1 and S3). The crystal structure of $[\mathbf{L6}]^+$ reveals that the three connected heterocycles of the bis(benzimidazole)pyridine (bzimpy) binding unit adopt pseudo-twofold *transoid-transoid* arrangements of the nitrogen donor

atoms (Figures 2 and S1 and Tables S1-S3). The cyanine segment in [**L6**]$^{+}$ is connected to the phenyl substituted bzimpy binding site through a sulfur atom, where the C-S-C angle amounts to 100.3(1)°, as expected for organic sulfides.[19] Reaction of stoichiometric amounts of [**L6**](PF_6) (1.0 eq.) and [Er(hfa)$_3$dig] (hfa = hexafluoroacetylacetonate and dig = 1-methoxy-2-(2-methoxyethoxy)ethane; 1.0 eq.) in dichloromethane/acetonitrile followed by dropwise addition of *tert*-butyl methyl ether yielded 63% of microcrystalline powders for which the elemental analysis was compatible with the formation of the [**L6**Er(hfa)$_3$](PF_6)·2.0CH_3CN·1.9$C_5H_{12}O$ complex. Slow diffusion of diethyl ether into a concentrated dichloromethane solution of the latter complex under aerobic condition provided X-ray quality crystals of [**L6**Er(hfa)$_2$(O_2CCF_3)](PF_6)·(CH_3CH_2)$_2$O (Figure 2, Tables S4-S6 and Figure S2), in which the trifluoroacetate anion is produced by retro-Claisen condensation of one hfa$^-$ ligand in the presence of water traces during the long crystallization process.[20] The crystal structure of [**L6**Er(hfa)$_2$(O_2CCF_3)](PF_6)·(CH_3CH_2)$_2$O confirms the nine-coordination around the erbium cation by the three nitrogen atoms of the meridionally bound bzimpy of the ligand [**L6**]$^{+}$ and the six oxygen atoms of two didentate hexafluoroacetylacetonate co-ligands and of one didentate trifluoroacetate anions. The [ErN_3O_6] chromophore adopts a C_s-symmetrical distorted muffin shape (Shape's scores are given in the experimental section, Supporting Information). Upon complexation, the C-S-C angle in coordinated [**L6**]$^{+}$ ligand slightly increases and reaches 105.5(3)°, whereas the interplanar angle between the pyridine and the bridging phenyl rings decreases with respect to the values observed for the free ligand.

Solution behavior and thermodynamic speciation of [L6Er(hfa)$_3$]$^{+}$. ^{1}H NMR titration of millimolar concentrations of [**L6**](PF_6) ligand with diamagnetic [Y(hfa)$_3$dig] (the size of Y^{3+} is close to that of Er^{3+}) in CD_2Cl_2 at room temperature revealed the formation of [**L6**Y(hfa)$_3$]$^{+}$ as the only complex; a host-guest exchange reaction which can be modeled with equilibrium 1 (Figures 3 and S4-S5).

$$[\mathbf{L6}]^{+} + [\mathrm{Y(hfa)_3dig}] \rightleftharpoons [\mathbf{L6}\mathrm{Y(hfa)_3}]^{+} + \mathrm{dig} \qquad \beta_{1,1,\mathrm{exch}}^{[\mathbf{L6}]^{+},\mathrm{Y(hfa)_3}} \qquad (1)$$

Although the NMR signals of the cyanine segment in [**L6**]$^+$ are mainly unaffected upon complexation (Figures 3, S4 and S5), the upfield shift of H3 and the downfield shift of H4 in the diamagnetic complex [**L6**Y(hfa)$_3$]$^+$ are diagnostic for the binding of the bzimpy moiety to the metal (numbering scheme in Figure 2).[21]

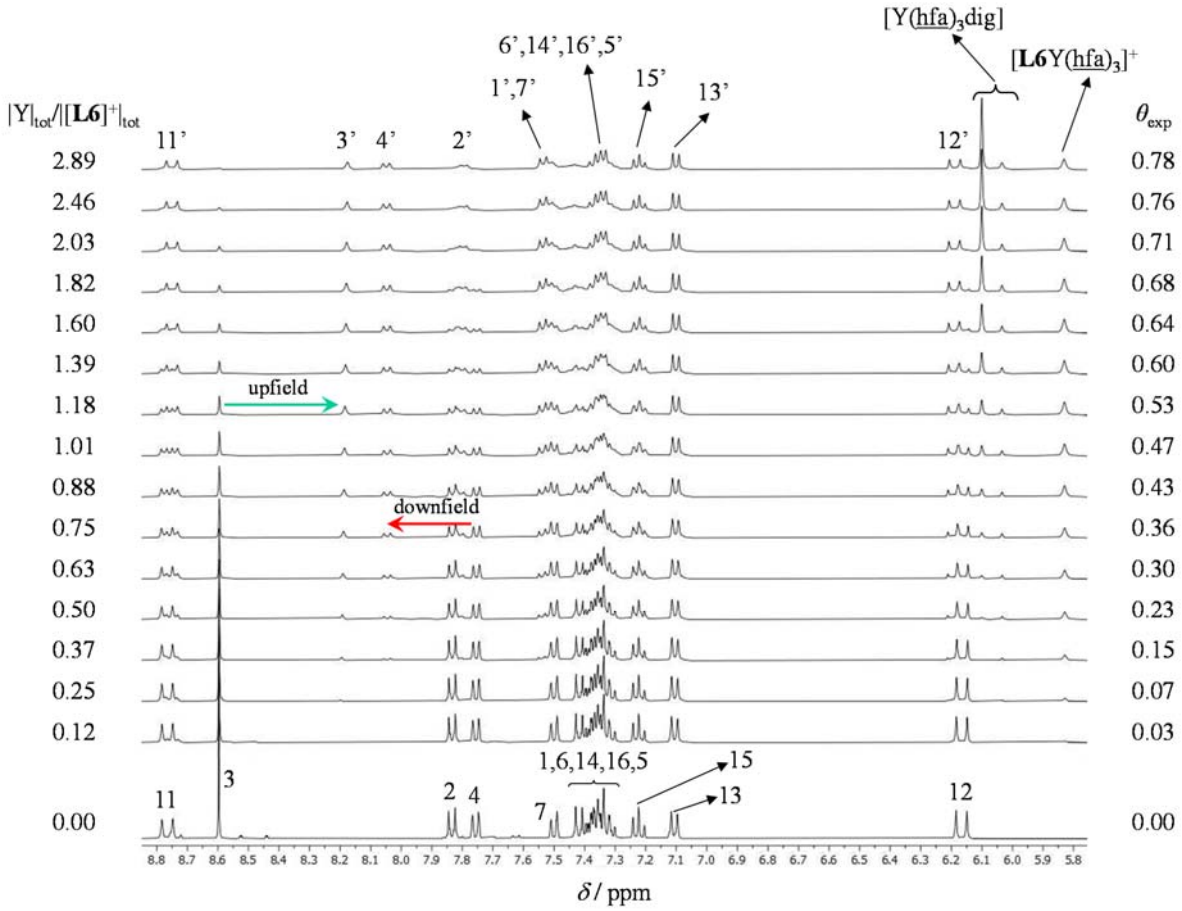

Figure 3. ^{1}H NMR spectra recorded upon titration of [**L6**](PF$_6$) with [Y(hfa)$_3$dig] in CD_2Cl_2 + 0.14 M diglyme at 293 K ($3\cdot10^{-3} \le |[\mathbf{L6}]^+|_{tot} \le 5\cdot10^{-3}$ M and $5\cdot10^{-4} \le |Y|_{tot} \le 1\cdot10^{-2}$ M). The numbering is taken from Figure 2. Numbers with prime (') symbol correspond to the signals arising upon formation of [**L6**Y(hfa)$_3$]$^+$ complex. The occupancy factors (Equation 3) are shown on the right.

To have a reliable access to the stability constant $\beta_{1,1,exch}^{[\mathbf{L6}]^+,Y(hfa)_3}$ introduced in eq. 1, the latter ^{1}H NMR titration was repeated in the presence of a constant total concentration of diglyme (0.14 M) for fixing the activity coefficients,[22] which transforms eq. 1 into the conditional association process summarized in eq. 2 (Figure 3).

$$[\mathbf{L6}]^+ + [Y(hfa)_3] \rightleftharpoons [\mathbf{L6}Y(hfa)_3]^+ \qquad \beta_{1,1,cond}^{[\mathbf{L6}]^+,Y(hfa)_3} = \beta_{1,1,exch}^{[\mathbf{L6}]^+,Y(hfa)_3} / |dig|_{tot} \qquad (2)$$

Integrations of the signals of the same proton in the free ligand $[\mathbf{L6}]^+$ ($I^{H}_{\mathbf{L6}}$) and in the complex $[\mathbf{L6}Y(hfa)_3]^+$ ($I^{H}_{\mathbf{L6}Y}$) provide the experimental occupancy factors $\theta^{Y}_{[\mathbf{L6}]^+}$ along the titration process together with the free concentration of metal $\left|Y(hfa)_3\right| = \left|Y\right|_{tot} - \theta^{Y}_{[\mathbf{L6}]^+}\left|[\mathbf{L6}]^+\right|_{tot}$ (left and central parts of eqn 3). The resulting plot of $\theta^{Y}_{[\mathbf{L6}]^+}$ *versus* $\left|Y(hfa)_3\right|$ (Figure S6) can be fitted to the standard Langmuir binding isotherms (right part of eqn 3) to give the thermodynamic constant $\beta^{[\mathbf{L6}]^+,Y(hfa)_3}_{1,1,cond}$ = 414(56) (equilibrium 2), which transforms into $\beta^{[\mathbf{L6}]^+,Y(hfa)_3}_{1,1,exch} = \beta^{[\mathbf{L6}]^+,Y(hfa)_3}_{1,1,cond}\left|dig\right|_{tot}$ = 60(8) (equilibrium 1).

$$\theta^{Y}_{[\mathbf{L6}]^+} = \frac{\left|Y(hfa)_3\right|_{bound}}{\left|[\mathbf{L6}]^+\right|_{tot}} = \frac{I^{H}_{\mathbf{L6}Y}}{I^{H}_{\mathbf{L6}Y} + I^{H}_{\mathbf{L6}}} = \frac{\left|Y\right|_{tot} - \left|Y(hfa)_3\right|}{\left|[\mathbf{L6}]^+\right|_{tot}} = \frac{\beta^{[\mathbf{L6}]^+,Y(hfa)_3}_{1,1,cond}(\left|Y(hfa)_3\right|)}{1 + \beta^{[\mathbf{L6}]^+,Y(hfa)_3}_{1,1,cond}(\left|Y(hfa)_3\right|)} \quad (3)$$

As expected for the binding of a positively charged ligand to a neutral lanthanide container, the latter value $\beta^{[\mathbf{L6}]^+,Y(hfa)_3}_{1,1,exch}$ = 60(8) is approximately four times smaller than the constant $\beta^{\mathbf{L4},Y(hfa)_3}_{1,1,exch}$ = 271(57) measured for the formation of $[\mathbf{L4}Y(hfa)_3]$ in dichloromethane, where **L4** is the analogue of **L6** but without the positively charged dye (Figure 1d).[23] Taking (i) $\beta^{[\mathbf{L6}]^+,Y(hfa)_3}_{1,1,exch}$ = 60(8) as a valuable estimation of the stability constant of the analogous erbium complex and (ii) $|Er|_{tot} = |[\mathbf{L6}]^+|_{tot} = 5\cdot10^{-4}$ M as the condition used for conducting the photophysical measurements, one can calculate that $\left|[\mathbf{L6}Er(hfa)_3]^+\right|$ = 4.43·10^{-4} M and the desired $[\mathbf{L6}Er(hfa)_3]^+$ complex stands for more than 88% of the ligand speciation in solution. The latter claim was confirmed by the absence of significant signal arising from free ligand in the ^{1}H NMR spectrum recorded for $[\mathbf{L6}Y(hfa)_3]^+$ in 5·10^{-4} M solution (Figure S7a). Repeating the latter experiment in acetonitrile confirms that the latter speciation is maintained in this solvent (Figure S7b), which is used for recording the photophysical data.

Photophysical characterizations of $[\mathbf{L6}]^+$ and $[\mathbf{L6}Er(hfa)_3]^+$. The electronic absorption spectrum of the free ligand $[\mathbf{L6}]^+$ in acetonitrile solution (red trace in Figure 4a) displays two major bands located in the ultraviolet (UV) at 32154 cm^{-1} (311 nm, ε = 56247 M^{-1}·cm^{-1}) and in the NIR domain at 12579 cm^{-1} (795 nm, ε = 233323 M^{-1}·cm^{-1}). In line with the absorption spectra taken separately for

L4[24] and for the [IR-806]$^+$ cyanine dye,[25] the absorption bands observed in [**L6**]$^+$ can be assigned to (i) π_2*←π transitions located on the bzimpy binding site at high energy and (ii) π_1*←π located on the NIR cyanine part at low energy (Scheme 1a).

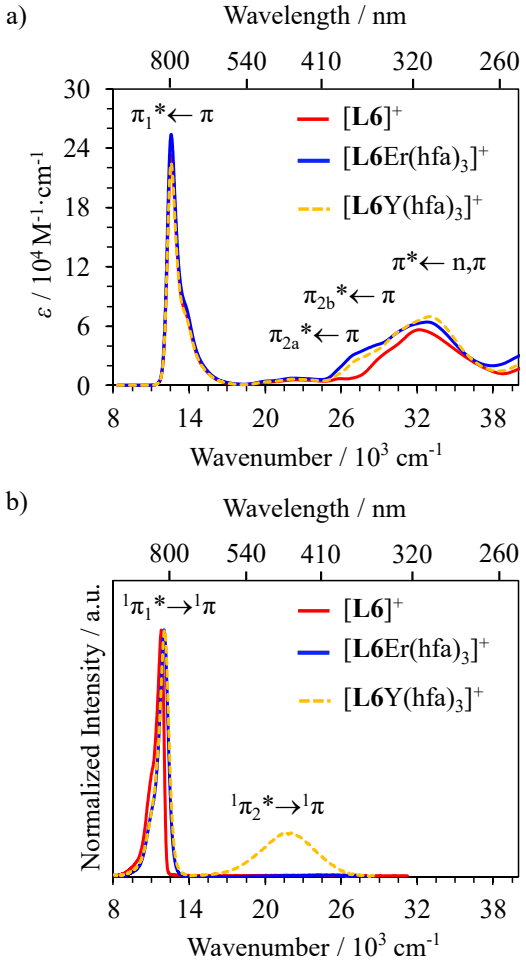

Figure 4. a) Absorption and b) emission (λ_{exc} = 310 nm, $\tilde{\nu}_{exc}$ = 32258 cm^{-1}) spectra of the ligand [**L6**]$^+$ and the [**L6**Ln(hfa)$_3$]$^+$ (Ln = Er and Y) complexes in acetonitrile solution (|[**L6**]$^+$| = 5·10^{-4} M and |[**L6**Ln(hfa)$_3$]$^+$| = 4·10^{-4} M for absorption; |[**L6**]$^+$| = 3·10^{-5} M and |[**L6**Ln(hfa)$_3$]$^+$| = 5·10^{-4} M for emission) at 293K. The energies of the peaks and their absorption coefficients are given in the main text.

Excitation of the ligand [**L6**]$^+$ into the π_2*←π transition at 310 nm in acetonitrile (293 K) yields a single broad emission band in the NIR domain, for which the maximum is located at 848 nm (11792 cm^{-1}, red trace in Figure 4b). The lack of any emission in the UV-Visible domain suggests the operation of efficient internal conversion process between the energy levels located on the two

chromophore segments in [**L6**]$^{+}$. Moreover, the same NIR emission band (848 nm) can be recorded upon excitation of [**L6**]$^{+}$ into the high-energy edge of π_1*←π absorption band (λ_{exc} = 640 nm in acetonitrile at 293 K, Figure S8) in agreement with its assignment to the $^1\pi_1$*→$^1\pi$ transitions of the cyanine segment (787 cm^{-1} Stokes shift with respect to the maximum of its $^1\pi_1$*←$^1\pi$ absorption band, Scheme 1a).

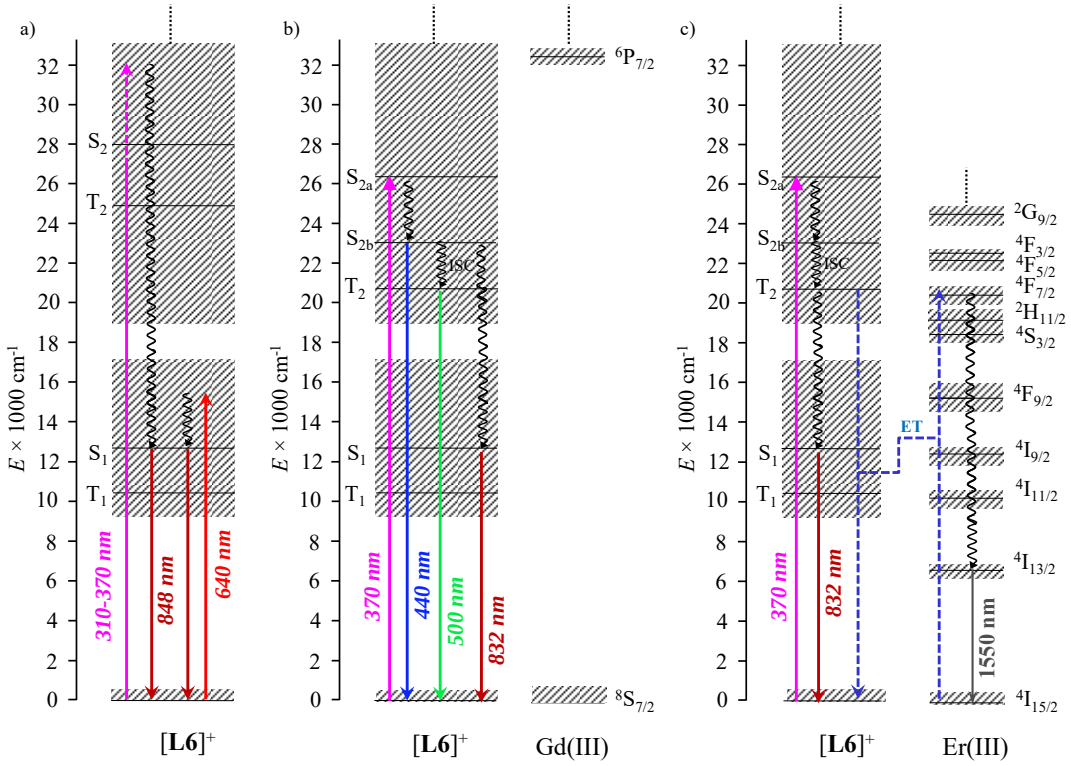

Scheme 1. Simplified Jablonski diagram established for a) [**L6**]$^{+}$, b) [**L6**Gd(hfa)$_3$]$^{+}$ and c) [**L6**Er(hfa)$_3$]$^{+}$ illustrating the possible mechanisms for inducing light downshifting (ISC = intersystem crossing, straight upward arrows = excitation processes, dashed arrows = non-radiative sensitizer-to-activator energy-transfer processes, undulating arrows = non-radiative multiphonon relaxation and straight downward arrows = radiative emission processes). The approximate energy of T_1 as well as the energies of erbium-centered excited levels have been extracted from the literature.[12,24] The hfa-based electronic levels in the complexes are omitted for clarity.

Upon complexation of the ligand to Ln^{3+} in [**L6**Ln(hfa)$_3$]$^{+}$ (Ln = Y, Gd, Er) at 5·10^{-4} M in acetonitrile (more than 88% of the ligand speciation corresponds to the target complex), the bzimpy-centered π_2*←π transition undergoes the well-known π_{2a}*,π_{2b}*←π splitting accompanying the *trans-trans*→*cis-cis* rearrangement of the aromatic tridentate binding unit (Scheme 1b), a spectral feature

diagnostic for the coordination of the bzimpy binding site to the central metallic center (blue and dashed yellow traces in Figure 4a).[23] Additionally, the absorption spectrum of [**L6**Ln(hfa)$_3$]$^+$ shows bands centered at ~ 33400 cm^{-1} (λ ~ 300 nm) which are characteristics for coordinated hfa$^-$ anion and assigned to the spin-allowed $\pi^*\leftarrow$n,π transitions centered on these co-ligands.[23] As expected, the low energy NIR band observed in the absorption spectrum of free [**L6**]$^+$ ligand originating from the cyanine-centered $\pi_1^*\leftarrow\pi$ transitions remain intact upon complexation in [**L6**Ln(hfa)$_3$]$^+$ (Figure 4a).

Excitation of [**L6**Y(hfa)$_3$]$^+$ in solution at room temperature into the ligand-centered $\pi_{2b}^*\leftarrow\pi$ transition at 310 nm (32260 cm^{-1}) shows (i) a strong ligand-centered emission band in the NIR range at 832 nm (12019 cm^{-1}) similar to that observed for the free ligand upon UV excitation but blue-shifted by 227 cm^{-1} (dashed yellow traces in Figures 4b and S8) together with (ii) an additional broad emission band in the visible part at 440 nm (22730 cm^{-1}) which can be assigned to the residual bzimpy-centered singlet $^1\pi_{2b}^*\rightarrow{}^1\pi$ emission (dashed yellow trace in Figure 4b). Excitation of [**L6**Gd(hfa)$_3$]$^+$ in the 310-370 nm range provided emission spectra very similar to those previously discussed for [**L6**Y(hfa)$_3$]$^+$, but the combination of heavy-atom effect[26] and of paramagnetic coupling[27] with Ln = Gd(III) lead to some boosted additional long-lived ligand-centered triplet emissions $^3\pi_2^*\rightarrow{}^1\pi$ emission at 500 nm (20000 cm^{-1}, 0-0 transition detected in frozen acetonitrile solution at 10 K, Figure S9) originating from the tridentate bzimpy unit. Due to instrumental limitations, we could not record the emission of cyanine-centered triplet state in [**L6**Gd(hfa)$_3$]$^+$, the energy of which is expected to be located around 981 nm (10194 cm^{-1}) as previously reported for the triplet state of closely related [IR-806]$^+$ cyanine dye antenna attached to optically inert $NaGdF_4$ nanoparticles (Scheme 1b).[12]

The latter visible bzimpy-based emission bands are lacking in [**L6**Er(hfa)$_3$]$^+$ due to quenching by efficient intramolecular **L6**$\rightarrow$Er energy transfers (ET) involving the excited levels of the open-shell metal and of the organic chromophore, but the dye-based NIR emission at 832 nm is maintained (blue trace in Figure 4b and Scheme 1c). Finally, UV ligand-centered excitation of solid samples of [**L6**Er(hfa)$_3$](PF_6) at room temperature showed that the broad ligand-centered NIR emission (Figure S8) is accompanied by the characteristic, but very weak downshifted Er($^4I_{13/2}\rightarrow{}^4I_{15/2}$) luminescence

at 1550 nm (6450 cm^{-1}); a strong support for the operation of **L6**→Er energy transfers occurring in the [**L6**Er(hfa)$_3$]$^+$ chromophore (Figure S10 and Scheme 1c). For [**L6**Er(hfa)$_3$]$^+$ in acetonitrile, the low-energy Er($^4I_{13/2}$→$^4I_{15/2}$) emission band is very weak and difficult to be exploited accurately (Figure S11). Altogether, the absorption spectra point to a rather negligible perturbation of the electronic levels of the cyanine dye and of the tridentate binding units in the phenyl-sulfur bridged version of these chromophores as they exist in the [**L6**]$^+$ receptor. The emission spectra indicate that non-radiative internal relaxation pathways allow the energy to migrate from the tridentate aromatic part toward the cyanine dye, a process boosted in the open-shell [**L6**Er(hfa)$_3$]$^+$ complex.

Ligand-sensitized upconversion operating in [L6Er(hfa)$_3$]$^+$. Continuous NIR diode laser excitation at 801 nm of [**L6**Er(hfa)$_3$]$^+$ ($5\cdot10^{-4}$ M in acetonitrile at room temperature) does not exhibit well-defined downshifted NIR Er($^4I_{13/2}$→$^4I_{15/2}$) emission (Figure S11), but two upconverted emission bands can be detected in the visible region centered at 542 nm (18450 cm^{-1}) and 522 nm (19157 cm^{-1}), which are unambiguously assigned to the erbium-centered Er($^4S_{3/2}$→$^4I_{15/2}$) and Er($^2H_{11/2}$→$^4I_{15/2}$) transitions, respectively (Figure 5a). The corresponding log(I_{up})-log(P) plot (I_{up} = intensity of upconverted emission and P = incident pump intensity) reveals a linear dependence of the emission on the incident pump intensity with a slope of 1.51(4), which is compatible with the successive absorption of two NIR photons prior to reach the Er^{3+}-centered emissive excited levels (Figure 5b and Scheme 2); one of the characteristics of linear light upconversion processes.[10,28] The lack of upconverted emission following 801 nm NIR laser excitation in absence of dye but with erbium in the [Er(hfa)$_3$dig] complex in acetonitrile solution at room temperature (Figure S12) together with the lack of any upconverted emissions following NIR laser excitation in absence of erbium and in presence of the dye in [**L6**Y(hfa)$_3$]$^+$, as well as in free [**L6**]$^+$ ligand at 801 nm (acetonitrile, 293 K, Figures S12) discard the operation of competitive ligand-centered non-linear two-photon absorption processes.[29] Moreover, considering the negligible molar extinction coefficient of the forbidden metal-centered Er($^4I_{9/2}$←$^4I_{15/2}$) transition (ε_{801}^{Er} = 0.12 $M^{-1}\cdot cm^{-1}$)[24] compared with that of the allowed ligand-centered π*←π transition in [**L6**Er(hfa)$_3$]$^+$ at 801 nm ($\varepsilon_{801}^{[\mathbf{L6}]^+}$ = $2.4\cdot10^5$ $M^{-1}\cdot cm^{-1}$), it can be reasonably

claimed that the erbium-centered intermediate excited levels are pumped dominantly through the ligand-centered excitation pathway (① in Scheme 2) rather than through the competitive erbium-centered Er($^4I_{9/2}$←$^4I_{15/2}$) excitation channel (② in Scheme 2).

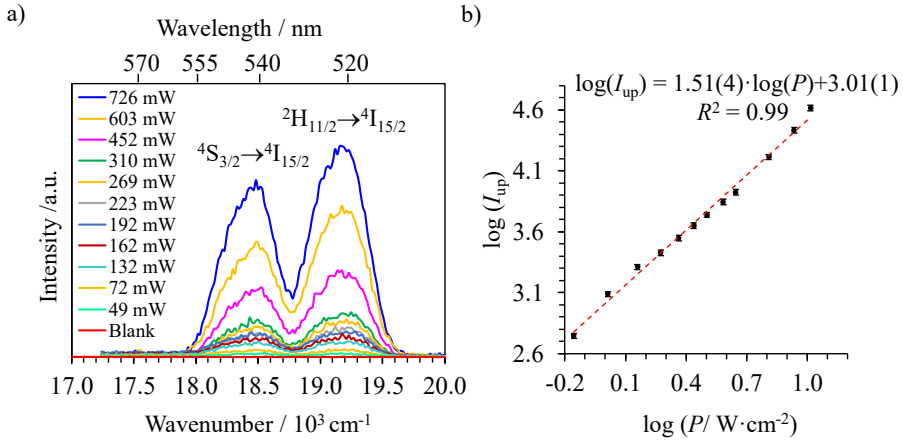

Figure 5. a) Upconverted visible Er($^2H_{11/2}$→$^4I_{15/2}$) and Er($^4S_{3/2}$→$^4I_{15/2}$) emissions observed for [**L6**Er(hfa)$_3$]$^+$ recorded in acetonitrile solution ($5\cdot10^{-4}$ M, 293 K) upon laser excitation at λ_{exc} = 801 nm ($\tilde{\nu}_{exc}$ = 12284 cm^{-1}) and using increasing incident pump intensities focused on a spot size of ≈ 0.07 cm^2 (the blank was recorded upon irradiation of the pure acetonitrile at P = 5.1 W·cm^{-2}) and b) corresponding log-log plot of upconverted intensities I_{up} as a function of incident pump intensities P (in W·cm^{-2}). The energies of the peaks are given in the main text.

Although the pertinent Jablonski diagram depicted in Scheme 2 highlights the spectral overlap of both singlet and triplet states of the ligand with the Er^{3+}-centered intermediate Er($^4I_{9/2}$) and Er($^4I_{11/2}$) levels, it is of interest to estimate the extent to which the long-lived triplet state populates the metal-centered levels (yellow dashed lines in Scheme 2) with respect to short-lived singlet state (blue dashed lines in Scheme 2). To qualitatively address this challenge, the intensity of upconverted emission has been monitored in the absence and in the presence of molecular dioxygen, which is known to act as an efficient quencher of the triplet state population (Figure S13).[30] The lack of perceptible difference for the intensity of upconversion signals recorded for [**L6**Er(hfa)$_3$]$^+$ in solution with or without dioxygen suggests that ligand-centered singlet state is the dominant sensitizing level for feeding Er^{3+}-centered excited states via energy transfer processes.

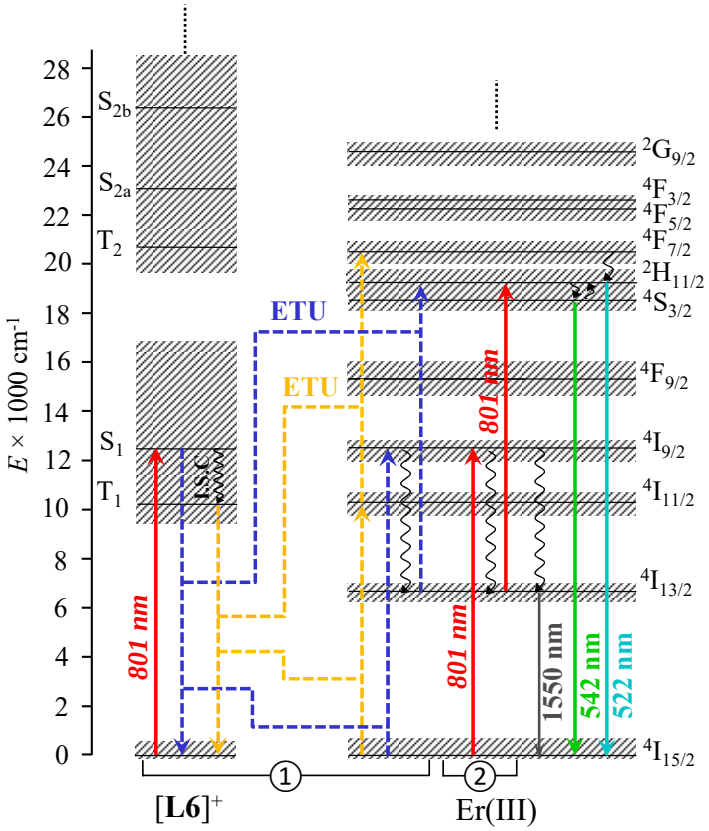

Scheme 2. Jablonski diagram established for [**L6**Er(hfa)$_3$]$^+$ and illustrating the possible mechanisms for inducing light upconversion through ① ligand-sensitized energy transfer upconversion (ETU) and ② erbium-centered excited state absorption (ESA) upon 801 nm excitation (ISC = intersystem crossing, straight upward arrows = excitation processes, dashed arrows = non-radiative sensitizer-to-activator energy-transfer processes, undulating arrows = non-radiative multiphonon relaxation and straight downward arrows = radiative emission processes). The approximate energy of T_1 as well as the energies of erbium-centered excited levels have been extracted from the literature.[12,24]

Since these cyanine dyes are known to suffer from photodegradation,[31] a phenomenon previously detected when they are employed as NIR sensitizers for UCNPs,[6c,14,32] the photostability of [**L6**Er(hfa)$_3$]$^+$ in solution have been investigated by recording the changes in the absorption as well as in the upconverted emission spectra upon continuous laser irradiation at a constant excitation power density (5.7 W·cm^{-2}, Figure S14). As expected, a stepwise decrease in intensity is observed in the dye-centered absorption spectrum (= NIR part) concomitant with a gradual solution color change from green to orange, while the high-energy absorption bands (= UV part) of the [**L6**Er(hfa)$_3$]$^+$ associated with electronic transitions located on the bound multidentate coordinating units, remains

fairly intact (Figure S14a). Conversely, the intensity of upconverted signal increases systematically by continuing the laser irradiation of the sample, which points the impairment of self-quenching processes upon 'optical dilution' of sample due to photocleavage of the cyanine dye moiety in [**L6**Er(hfa)$_3$]$^+$ (Figure S14b). Since such self-quenching processes reach their greatest extent in concentrated solution or in the solid state,[33] the faint upconverted signal recorded in these conditions strongly supports this analysis (Figure S15).

$$\frac{\Phi_{up}}{\Phi_{ref}} = \frac{E_{up}}{E_{ref}} \cdot \frac{A_{ref}}{A_{up}} \cdot \frac{{n_{ref}}^2}{{n_{up}}^2} \cdot \frac{P_{exc,ref}}{P_{exc,up}} \cdot \frac{h\nu_{exc,up}}{h\nu_{exc,ref}} \quad (4)$$

Finally, the upconversion process operating in [**L6**Er(hfa)$_3$]$^+$ has been quantified through the estimation of its quantum yield by using the relative method formulated in eqn 4 and with the help of indocyanine green as the reference[34] (Φ is the quantum yield, E is the integrated emission spectrum, A is the absorbance at the excitation wavelength and $h\nu_{exc}$ is the energy of the incident photon at frequency $\nu_{exc} = (c/\lambda_{exc})$ so that $I_{exc} = P_{exc}/h\nu_{exc}$ is the spectral radiant power measuring the incident excitation intensity; see details in the Supporting Information).[10b,35] Although the ligand-sensitized upconversion quantum yield $\Phi_{up} = 1.9(2)\cdot10^{-10}$ ($P_{exc} = 1.4$ W·cm^{-2}) calculated for [**L6**Er(hfa)$_3$]$^+$ is comparable with $\Phi_{up} = 1.2(6)\cdot10^{-10}$ ($P_{exc} = 1.4$ W·cm^{-2}) reported for the ESA mechanism operating in [Er(**L4**)$_3$]$^{3+}$,[10b] the associated values of the upconversion brightness $B = \Phi(\lambda)\times\varepsilon(\lambda)$, where $\varepsilon(\lambda)$ is the molar absorption coefficient at the excitation wavelength λ,[36] reveals an enhancement up to 6 orders of magnitude in going from B([Er(**L4**)$_3$]$^{3+}$) = $1(1)\cdot10^{-11}$ to B([**L6**Er(hfa)$_3$]$^+$) = $5(1)\cdot10^{-5}$.

Conclusions

The connection of a NIR dye antenna to a tridentate bzimpy binding unit results in the ligand [**L6**]$^+$ which can (very) efficiently capture NIR photons. The replacement of diglyme (dig) in [Er(hfa)$_3$dig] with ligand [**L6**]$^+$ leads to the formation of a stable [**L6**Er(hfa)$_3$]$^+$ complex which represents approximately 90% of ligand speciation in solution. Its X-ray structure confirms the binding of [**L6**]$^+$ to Er^{3+} with the existence of a low-symmetry nine-coordinate [ErN$_3$O$_6$] chromophore. Low-power NIR laser excitation of the [**L6**Er(hfa)$_3$]$^+$ complex at 801 nm (NIR) in non-deuterated acetonitrile

solution at room temperature produces upconverted erbium-centered emission signals at 542 nm and 522 nm (visible). The associated Jablonski diagrams built for the mononuclear [**L6**Er(hfa)$_3$]$^+$ complex supports the operation of ligand-sensitized energy transfer upconversion (ETU) mechanism for inducing NIR-to-visible light upconversion. The high NIR absorption cross section of the cyanine dye in [**L6**]$^+$ boosts the upconversion brightness of discrete [**L6**Er(hfa)$_3$]$^+$ complex by six orders of magnitude compared with related [Er(**L4**)$_3$]$^{3+}$ molecular systems. Although widely used in UCNPs, the smart idea of exploiting NIR dye sensitization in the field of metal-based molecular upconversion also overcomes the inherent low quantum yields due to fast non-radiative processes thanks to efficient light-harvesting processes. In addition, the tunability of molecular objects offers plenty of room for further improving the upconversion efficiency in such systems to push molecular upconversion toward the range of practical applications. In this line, increasing the number of dye-sensitizers per a single metal activator as well as optimizing the efficiency of energy transfer through tailoring the ligand structure are currently under investigations.

ASSOCIATED CONTENT

Supporting Information

The Supporting Information is available free of charge at https://pubs.acs.org/doi/XXX.

Complete experimental details, photophysical data (PDF).

X-ray data for [**L6**](PF$_6$) and [**L6**Er(hfa)$_2$(O$_2$CCF$_3$)](PF$_6$)·(CH$_3$CH$_2$)$_2$O (CIF). CCDC 2091958-2091959 contain the supplementary crystallographic data. These data can be obtained free of charge from the Cambridge Crystallographic Data Centre via www.ccdc.cam.ac.uk/

AUTHOR INFORMATION

Corresponding Authors

Bahman Golesorkhi, *Department of Inorganic and Analytical Chemistry. University of Geneva, 30 quai E. Ansermet CH-1211 Geneva 4 (Switzerland) and Department of Chemistry, University of*

California, Berkeley, Berkeley, California 94720 (United States); Email: bahman.golesorkhi@berkeley.edu

Claude Piguet, *Department of Inorganic and Analytical Chemistry. University of Geneva, 30 quai E. Ansermet CH-1211 Geneva 4 (Switzerland)*; Email: claude.piguet@unige.ch

Authors

Soroush Naseri, *Department of Inorganic and Analytical Chemistry. University of Geneva, 30 quai E. Ansermet CH-1211 Geneva 4 (Switzerland).*

Inès Taarit, *Department of Inorganic and Analytical Chemistry. University of Geneva, 30 quai E. Ansermet CH-1211 Geneva 4 (Switzerland).*

Filipe Alves, *Department of Inorganic and Analytical Chemistry. University of Geneva, 30 quai E. Ansermet CH-1211 Geneva 4 (Switzerland).*

Laure Guénée, *Laboratory of Crystallography. University of Geneva, 24 quai E. Ansermet. CH-1211 Geneva 4 (Switzerland).*

Homayoun Nozary, *Department of Inorganic and Analytical Chemistry. University of Geneva, 30 quai E. Ansermet CH-1211 Geneva 4 (Switzerland)*.

Present Address

Bahman Golesorkhi, *Department of Chemistry, University of California, Berkeley, Berkeley, California 94720 (United States).*

Notes

The authors declare no conflict of interest.

ACKNOWLEGMENTS

This work is supported through grants from the Swiss National Science Foundation (grant 200020_178758).

REFERENCES

1 a) Bloembergen, N., Solid State Infrared Quantum Counters. *Phys. Rev. Lett.* **1959**, *2*, 84-85; b) Porter, J. F., Fluorescence Excitation by Absorption of Two Consecutive Photons. *Phys.*

Rev. Lett. **1961**, *7*, 414-415; c) Parker, C. A.; Hatchard, C. G., Sensitized Anti-Stokes Delayed Fluorescence. *Proc. Chem. Soc.* **1962**, 386-387; d) Parker, C. A., Sensitized P-Type Delayed Fluorescence. *Proc. R. Soc. London, Ser. A* **1963**, *276*, 125-135.

2 a) Auzel, F., Upconversion and Anti-Stokes Processes with f and d Ions in Solids *Chem. Rev.* **2004**, *104*, 139-173; b) van der Ende, B. M.; Aarts, L.; Meijerink, A., Lanthanide Ions as Spectral Converters for Solar Cells. *Phys. Chem. Chem. Phys.* **2009**, *11*, 11081-11095.

3 a) Gamelin, D. R.; Güdel, H.-U., Design of Luminescent Inorganic Materials: New Photophysical Processes Studied by Optical Spectroscopy. *Acc. Chem. Res.* **2000**, *33*, 235-242; b) Haase, M.; Schäfer, H., Upconverting Nanoparticles. *Angew. Chem. Int. Ed.* **2011**, *50*, 5808-5829; c) Ramasamy, P.; Manivasakan, P.; Kim, J. Y., Upconversion Nanophosphors for Solar Cell Applications. *RSC Adv.* **2014**, *4*, 34873-34895.

4 a) Auzel, F., Compteur Quantique par Transfert d'Energie entre deux Ions de Terres Rares dans un Tungstate Mixte et dans un Verre. *C. R. Acad. Sc. Paris* **1966**, *B262*, 1016-1019; b) Auzel, F. Compteur Quantique par Transfert d'Energie de Yb(III) à Tm(III) dans un Tungstate Mixte et dans un Verre Germanate. *C. R. Acad. Sc. Paris* **1966**, *B263*, 819-821; c) Heer, S.; Kömpe, K.; Güdel, H.-U.; Haase, M., Highly Efficient Multicolour Upconversion Emission in Transparent Colloids of Lanthanide-Doped $NaYF_4$ Nanocrystals. *Adv. Mater.* **2004**, *16*, 2102-2105; d) Wang, F.; Liu, X., Recent Advances in the Chemistry of Lanthanide-doped Upconversion Nanocrystals. *Chem. Soc. Rev.* **2009**, *38*, 976-989.

5 a) Carnall, W. T.; Goodman, G. L.; Rajnak, K.; Rana, R. S., A Systematic Analysis of the Spectra of the Lanthanides Doped into Single Crystal LaF_3. *J. Chem. Phys.* **1989**, *90*, 3443-3457; b) DeLoach, L. D.; Payne, S. A.; Chase, L. L.; Smith, L. K.; Kway, W. L.; Krupke, W. F., Evaluation of Absorption and Emission Properties of Yb^{3+} doped Crystals for Laser Applications. *IEEE J. Quantum Electron.* **1993**, *29*, 1179-1191; c) Strohhöfer, C.; Polman, A., Absorption and Emission Spectroscopy in Er^{3+}-Yb^{3+} Doped Aluminum Oxide Waveguides. *Opt. Mater.* **2003,** *21*, 705-712.

6 a) Zou, W.; Visser, C.; Maduro, J. A.; Pshenichnikov, M. S.; Hummelen, J. C., Broadband Dye-sensitized Upconversion of Near-infrared Light. *Nat. Photonics* **2012**, *6*, 560-564; b) Chen, G.; Damasco, J.; Qiu, H.; Shao, W.; Ohulchanskyy, T. Y.; Valiev, R. R.; Wu, X.; Han, G.; Wang, Y.; Yang, C.; Ågren, H.; Prasad, P. N., Energy-Cascaded Upconversion in an Organic Dye-sensitized Core/Shell Fluoride Nanocrystal. *Nano Lett.* **2015**, *15*, 7400-7407; c) Garfield, D. J.; Borys, N. J.; Hamed, S. M.; Torquato, N. A.; Tajon, C. A.; Tian, B.; Shevitski, B.; Barnard, E. S.; Suh, Y. D.; Aloni, S.; Neaton, J. B.; Chan, E. M.; Cohen, B. E.; Schuck, P. J., Enrichment of Molecular Antenna Triplets Amplifies Upconverting Nanoparticle Emission. *Nat. Photonics* **2018**, *12*, 402-407; d) Bao, G.; Wen, S.; Lin, G.; Yuan, J.; Lin, J.; Wong, K.-L.; Bünzli, J.-C. G.; Jin, D., Learning from Lanthanide Complexes: The Development of Dye-lanthanide Nanoparticles and their Biomedical Applications. *Coord. Chem. Rev.* **2021,** *429*, 213642.

7 Aboshyan-Sorgho, L.; Besnard, C.; Pattison, P.; Kittilstved, K. R.; Aebischer, A.; Bünzli, J.-C. G.; Hauser, A.; Piguet, C., Near-Infrared to Visible Light Upconversion in a Molecular Trinuclear d-f-d Complex. *Angew. Chem. Int. Ed.* **2011**, *50*, 4108-4112.

8 Nonat, A.; Chan, C. F.; Platas-Iglesias, C.; Liu, Z.; Wong, W.-T.; Wong, W.-K.; Wong, K.-L.; Charbonnière, L. J., Room Temperature Molecular Upconversion in Solution. *Nat. Commun.* **2016**, *11978*.

9 a) Souri, N.; Tian, P.; Platas-Iglesias, C.; Wong, K.-L.; Nonat, A.; Charbonnière, L. J., Upconverted Photosensitization of Tb Visible Emission by NIR Yb Excitation in Discrete Supramolecular Heteropolynuclear Complexes *J. Am. Chem. Soc.* **2017**, *139*, 1456-1459; b) Nonat, A.; Bahamyirou, S.; Lecointre, A.; Przybilla, F.; Mély, Y.; Platas-Iglesias, C.; Camerel, F.; Jeannin, O.; Charbonnière, L. J., Molecular Upconversion in Water in heteropolynuclear Supramolecular Tb/Yb Assemblies. *J. Am. Chem. Soc.* **2019**, *141*, 1568-1576.

10 a) Golesorkhi, B.; Nozary, H.; Guénée, L.; Fürstenberg, A.; Piguet, C., Room-Temperature Linear Light Upconversion in a Mononuclear Erbium Molecular Complex. *Angew. Chem. Int.*

Ed. **2018**, *57*, 15172-15176; b) Golesorkhi, B.; Taarit, I.; Bolvin, H.; Nozary, H.; Jiménez, J.-R.; Besnard, C.; Guénée, L.; Fürstenberg, A.; Piguet, C., Molecular Light-upconversion: We Have Had a Problem! When Excited State Absorption (ESA) Overcomes Energy Transfer Upconversion (ETU) in Cr(III)/Er(III) Complexes. *Dalton Trans.* **2021**, *50*, 7955–7968.

11 a) Huang, X.; Han, S.; Huang, W.; Liu, X., Enhancing Solar Cell Efficiency: The Search for Luminescent Materials as Spectral Converters. *Chem. Soc. Rev.* **2013,** *42*, 173-201; b) Bünzli, J.-C. G.; Chauvin, A.-S., Lanthanides in Solar Energy Conversion, *Handbook on the Physics and Chemistry of Rare Earths*, Vol. 44 (Eds.: J.-C. G. Bünzli, V. K. Pecharsky), Elsevier North Holland: Amsterdam, 2014, pp 169-281.

12 Knighton, R. C.; Soro, L. K.; Lecointre, A.; Pilet, G.; Fateeva, A.; Pontille, L.; Francés-Soriano, L.; Hildebrandt, N.; Charbonnière, L. J., Upconversion in Molecular Hetero-nonanuclear Lanthanide Complexes in Solution. *Chem. Commun.* **2021**, *57*, 53-56.

13 Gálico, D. A.; Ovens, J. S.; Sigoli, F. A.; Murugesu, M., Room-Temperature Upconversion in a Nanosized {Ln_{15}} Molecular Cluster-aggregate. *ACS Nano* **2021**, *15*, 5580-5585.

14 Hyppänen, I.; Lahtinen, S.; Ääritalo, T.; Mäkelä, J.; Kankare, J.; Soukka, T., Photon Upconversion in a Molecular Lanthanide Complex in Anhydrous Solution at Room Temperature. *ACS Photonics* **2014**, *1*, 394-397.

15 a) Ito, A.; Meyer, T. J., The Golden Rule. Application for Fun and Profit in Electron Transfer, Energy Transfer, and Excited-state Decay. *Phys. Chem. Chem. Phys.* **2012**, *14* (40), 13731-13745; b) Ward, M. D., Mechanisms of Sensitization of Lanthanide(III)-based Luminescence in Transition metal/Lanthanide and Anthracene/Lanthanide Dyads. *Coord. Chem. Rev.* **2010**, *254*, 2634-2642; c) Tanner, P. A.; Zhou, L.; Duan, C.; Wong, K.-L., Misconceptions in Electronic Energy Transfer: Bridging the Gap Between Chemistry and Physics. *Chem. Soc. Rev.* **2018**, *47*, 5234-5265.

16 Dexter, D. L., A Theory of Sensitized Luminescence in Solids. *J. Chem. Phys.* **1953**, *21*, 836-850.

17 Weissman, S. I., Intramolecular Energy Transfer The Fluorescence of Complexes of Europium. **1942**, *10*, 214-217.

18 Ziessel, R. F.; Ulrich, G.; Charbonnière, L. J.; Imbert, C.; Scopelliti, R.; Bünzli, J.-C. G., NIR Lanthanide Luminescence by Energy Transfer from Appended Terpyridine-boradiazaindacene Dyes. *Chem. Eur. J.* **2006**, *12*, 5060-5067.

19 a) Cremlyn, R. J., *An Introduction to Organosulfur Chemistry*, Wiley, New York, 1996, ISBN: 978-0-471-95512-2, p. 48-52. b) Takao, I.; Shuzo, T.; Masao, K., The Molecular Structure of Dimethyl Sulfide. *Bull. Chem. Soc. Jpn.* **1977**, *50*, 2564-2567.

20 a) Drake, S. R.; Lyons, A.; Otway, D. J.; Williams, D. J., An Unexpected Product Derived from the Reaction of $TbCl_3(H_2O)_6$ and [Na(hfac)]: Synthesis, Characterization and X-ray Structure. *Inorg. Chem.* **1994**, *33*, 1230-1233; b) Zaïm, A.; Dalla Favera, N.; Guénée, L.; Nozary, H.; Hoang, T. N. Y.; Eliseeva, S. V.; Petoud, S.; Piguet, C., Lanthanide Hexafluoroacetylacetonates vs. Nitrates for the Controlled Loading of Luminescent Polynuclear Single-stranded Oligomers. *Chem. Sci.* **2013**, *4*, 1125-1136.

21 Lavallee, D. K.; Baughman, M. D.; Phillips, M. P., Comparisons of Proton and Carbon NMR Chemical Shifts for Low Spin d^6 Complexes of Pyridine and Substituted Pyridines as Probes of π Back-bonding. *J. Am. Chem. Soc.* **1977**, *99*, 718-724.

22 Baudet, K.; Kale, V.; Mirzakhani, M.; Babel, L.; Naseri, S.; Besnard, C.; Nozary, H.; Piguet, C., Neutral Heteroleptic Lanthanide Complexes for Unravelling Host-Guest Assemblies in Organic Solvents: The Law of Mass Action Revisited. *Inorg. Chem.* **2020**, *59*, 62-75.

23 Zaïm, A.; Nozary, H.; Guénée, L.; Besnard, C.; Lemonnier, J.-F.; Petoud, S.; Piguet, C., N-heterocyclic Tridentate Aromatic Ligands Bound to $[Ln(hfac)_3]$ Units: Thermodynamic, Structural and Luminescent Properties. *Chem. Eur. J.* **2012**, *18*, 7155-7168.

24 Golesorkhi, B.; Guénée, L.; Nozary, H.; Fürstenberg, A.; Suffren, Y.; Eliseeva, S. V.; Petoud, S.; Hauser, A.; Piguet, C., Thermodynamic Programming of Erbium(III) Coordination

Complexes for Dual Visible/Near-Infrared Luminescence. *Chem. Eur. J.* **2018**, *24*, 13158-13169.

25 a) Strekowski, L.; Lipowska, M.; Patonay, G., Substitution Reactions of a Nucleofugal Group in Heptamethine Cyanine Dyes. Synthesis of an Isothiocyanato Derivative for Labeling of Proteins with a Near-infrared Chromophore. *J. Org. Chem.* **1992**, *57*, 4578-4580; b) Tang, B.; Yu, F.; Li, P.; Tong, L.; Duan, X.; Xie, T.; Wang, X., A Near-infrared Neutral pH Fluorescent Probe for Monitoring Minor pH Changes: Imaging in Living HepG2 and HL-7702 Cells. *J. Am. Chem. Soc.* **2009**, *131*, 3016-3023.

26 Tobita, S.; Arakawa, M.; Tanaka, I., Electronic Relaxation Processes of Rare-Earth Chelates of Benzoyltrifluoroacetone. *J. Phys. Chem.* **1984**, *88*, 2697-2702.

27 Tobita, S.; Arakawa, M.; Tanaka, I., The Paramagnetic Metal Effect on the Ligand Localized S1-T1 Intersystem Crossing in the Rare-Earth-Metal Complexes with Methyl Salicylate. *J. Phys. Chem.* **1985**, *89*, 5649-5654.

28 Golesorkhi, B.; Fürstenberg, A.; Nozary, H.; Piguet, C., Deciphering and Quantifying Linear Light Upconversion in Molecular Erbium Complexes. *Chem. Sci.* **2019**, *10*, 6876-6885.

29 a) Andraud, C.; Maury, O., Lanthanide Complexes for Nonlinear Optics: from Fundamental Aspects to Applications. *Eur. J. Inorg. Chem.* **2009**, 4357-4371; b) Medishetty, R.; Zaręba, J. K.; Mayer, D.; Samoć, M.; Fischer, R. A., Nonlinear Optical Properties, Upconversion and Lasing in Metal-organic Frameworks. *Chem. Soc. Rev.* **2017**, *46*, 4976-5004.

30 a) Hübner, C. G.; Renn, A.; Renge, I.; Wild, U. P., Direct Observation of the Triplet Lifetime Quenching of Single Dye Molecules by Molecular Oxygen. *J. Chem. Phys.* **2001**, *115*, 9619-9622; b) Renn, A.; Seelig, J.; Sandoghdar, V., Oxygen-dependent Photochemistry of Fluorescent Dyes Studied at the Single Molecule Level. *Mol. Phys.* **2006**, *104*, 409-414.

31 Matikonda, S. S.; Helmerich, D. A.; Meub, M.; Beliu, G.; Kollmannsberger, P.; Greer, A.; Sauer, M.; Schnermann, M. J., Defining the Basis of Cyanine Phototruncation Enables a New

Approach to Single-Molecule Localization Microscopy. *ACS Cent. Sci.* **2021**, DOI 10.1021/acscebtsci.1c00483

32 Gorka, A. P.; Nani, R. R.; Zhu, J.; Mackem, S.; Schnermann, M. J., A Near-IR Uncaging Strategy Based on Cyanine Photochemistry. *J. Am. Chem. Soc.* **2014**, *136*, 14153-14159.

33 Fonin, A. V.; Sulatskaya, A. I.; Kuznetsova, I. M.; Turoverov, K. K., Fluorescence of Dyes in Solutions with High Absorbance. Inner Filter Effect Correction. *PLOS ONE* **2014**, *9*, e103878.

34 Rurack, K.; Spieles, M., Fluorescence Quantum Yields of a Series of Red and Near-Infrared Dyes Emitting at 600-1000 nm. *Anal. Chem.* **2011**, *83*, 1232-1242.

35 Wurth, C.; Grabolle, M.; Pauli, J.; Spieles, M.; Resch-Genger, U., Relative and Absolute Determination of Fluorescence Quantum Yields of Transparent Samples. *Nat. Protoc.* **2013**, *8*, 1535-1550.

36 Wong, K.-L.; Bünzli, J.-C. G.; Tanner, P. A., Quantum Yield and Brightness. *J. Lumin.* **2020**, *224*, 117256.

TOC

Low-power NIR excitation (801 nm) of a mononuclear molecular erbium complex equipped with an organic ligand capable of efficiently harvesting NIR photons resulted in green erbium-centered upconverted emission at room temperature in diluted solution.